

Transmission through multiple Mott insulator–semiconductor wells

Jan Verlage¹ and Peter Kratzer¹

¹*Fakultät für Physik and CENIDE, Universität Duisburg-Essen, Lotharstraße 1, 47057 Duisburg, Germany,*
(Dated: February 28, 2025)

Weakly and strongly interacting quantum many-body systems, namely semiconductors and Mott insulators, are combined into a layered heterostructure. Via the hierarchy of correlations, we derive and match the propagating quasi-particle solutions in the different regions and calculate the transmission coefficients through these layered structures. As a proof of principle, we find the well known transmission bands of a semiconductor heterostructure. Extending this idea to semiconductor and Mott insulator structures we calculate the transmittance and the resonance energies. Within a phase accumulation model we find analytical expressions for the scattering phase shift. Lastly, we find transmission curves with skewness for structures with applied voltage.

I. INTRODUCTION

Superlattices, engineered structures composed of alternating layers of different materials, have emerged as fascinating platforms for exploring novel electronic and optical properties. Their ability to exhibit unique phenomena, such as quantum confinement [1–3] and collective behavior, has captivated researchers in various disciplines. Traditionally, superlattices have been engineered predominantly from materials with well-defined metallic or semiconducting characteristics [4–6], e.g., GaAs/Al_xGa_{1-x}As [7, 8]. Moreover, they show energy filtering over potential barriers [9–12]. This plays a crucial role in applications including thermoelectric devices, photovoltaics or energy storage [13–15]. In the thermoelectric setting, a skewness of the transport distribution function is desired to simultaneously improve the different constituents, enhancing the thermoelectric power [16].

In contrast to semiconductor characteristics, Mott insulators [17, 18] are a class of materials characterized by their unusual behavior that defies conventional band theory. Standard band theory describes them as conductors, but the insulating behavior arises from strong electron-electron interactions that result in localized, rather than itinerant, electronic states [19, 20]. Mott insulators have been the subject of intense investigation for several decades, due to their relevance to a range of phenomena, including, for example, high-temperature superconductivity [21, 22]. In these materials, the transmission happens via quasi-particles showing distinct characteristics from usual semiconducting materials [23].

However, incorporating Mott insulators within the superlattice architecture, e.g. as ultra-thin silicide layers in silicon [24, 25], introduces an additional dimension of control through strong electron correlations. The strength of the Coulomb interaction between the electrons changes the size of the Mott gap. This effectively influences the transmission of electrons passing through these layers as doublon-holon quasi-particles. This allows for a better tailoring of the transmission characteristics compared to structures that lack this degree of freedom, and the Mott insulating layers introduce an additional

skewness of the transmission favorable in thermoelectric applications.

Usually the Mott behavior is treated within a DMFT framework which takes the individual layers as infinite dimensional [26, 27]. In this work, we use an approach via the hierarchy of correlations [28–30]. This method provides a powerful tool for describing both the weakly interacting semiconductors and strongly interacting Mott insulators on the same footing while maintaining spatial resolution.

The article is organized as follows; we first introduce the Hubbard model used as a theoretical description for the different material types as well as the hierarchy of correlations, the proof of concept involving superlattices constructed by different semiconductors is calculated afterwards and lastly the extension to semiconductor-Mott insulator heterostructures is made.

II. FERMİ-HUBBARD MODEL

In order to describe both the strongly correlated Mott insulating and the semiconductor sites we employ a tight-binding model, namely the Fermi Hubbard model [18, 31, 32]

$$\hat{H} = -\frac{1}{Z} \sum_{\mu\nu s} T_{\mu\nu} \hat{c}_{\mu s}^\dagger \hat{c}_{\nu s} + \sum_{\mu} U_{\mu} \hat{n}_{\mu}^{\uparrow} \hat{n}_{\mu}^{\downarrow} + \sum_{\mu s} V_{\mu} \hat{n}_{\mu s}. \quad (1)$$

This Hamiltonian describes the relevant band of the semiconductor, either valence or conduction band, with $U_{\mu} \equiv 0$, and the Mott insulator with non-zero on-site repulsion $U_{\mu} \neq 0$. Even if there is a small interaction in the semiconductor this is absorbed into an effective on-site potential V_{μ} similar to Fermi liquid theory [33, 34]. As usual, $\hat{c}_{\mu s}^\dagger$ and $\hat{c}_{\nu s}$ denote the fermionic creation and annihilation operators at the lattice sites μ and ν with spin $s \in \{\uparrow, \downarrow\}$ and $\hat{n}_{\mu s}$ are the associated number operators. The hopping matrix $T_{\mu\nu}$ encodes both the adjacency and the hopping strength. In the following, it is assumed in the form of nearest neighbor hopping and zero otherwise. Moreover, we assume a uniform hopping strength throughout the entire heterostructure, but the results can

be generalized to non-uniform hopping in a straightforward manner. The coordination number Z counts the nearest neighbors ν for any site μ and is assumed large, $Z \gg 1$. The different regions are differentiated by the two parameters, U_μ and V_μ . The Mott insulator is characterized by a large on-site repulsion $U \gg T$, creating the upper and lower Hubbard band, and zero on-site potential $V_\mu \equiv 0$. The semiconductor has an on-site potential $V_\mu \neq 0$, because only the relative positions of the semiconducting and Hubbard bands matter, and no on-site repulsion.

A. Hierarchy of Correlations

In the following we are interested in the propagation of electrons through heterostructures. Within the Mott insulating layers this propagation happens by quasi-particles, namely doublons $|\uparrow\downarrow\rangle$ in the upper Hubbard band and holons $|0\rangle$ in the lower Hubbard band on top of a half-filled background [23]. This is similar to the Hubbard-I approximation [18, 35]. To this end, we consider the reduced density matrices for one $\hat{\rho}_\mu$, two $\hat{\rho}_{\mu\nu}$ and more lattice sites. This is done by tracing out all other lattice sites but one, $\hat{\rho}_\mu = \text{tr}_\mu \hat{\rho}$. Additionally, we split up the correlations, $\hat{\rho}_{\mu\nu} = \hat{\rho}_\mu \hat{\rho}_\nu + \hat{\rho}_{\mu\nu}^{\text{corr}}$ and so on. From this starting point, we employ an expansion into powers of the inverse coordination number $1/Z$ based on the $Z \gg 1$ assumption. Doing so, higher order correlations are successively suppressed. While the two-site correlations scale as $\hat{\rho}_{\mu\nu}^{\text{corr}} = \mathcal{O}(1/Z)$, the three-sites ones scale as $\hat{\rho}_{\mu\nu\lambda}^{\text{corr}} = \mathcal{O}(1/Z^2)$ and so on. This hierarchy yields an iterative scheme for the correlations. Mathematically speaking, we start from the exact evolution equations for these correlations ($\hbar = 1$)

$$\begin{aligned} i\partial_t \hat{\rho}_\mu &= F_1(\hat{\rho}_\mu, \hat{\rho}_{\mu\nu}^{\text{corr}}), \\ i\partial_t \hat{\rho}_{\mu\nu}^{\text{corr}} &= F_2(\hat{\rho}_\mu, \hat{\rho}_{\mu\nu}^{\text{corr}}, \hat{\rho}_{\mu\nu\lambda}^{\text{corr}}), \end{aligned} \quad (2)$$

that we get from the Heisenberg equation. We now approximate them using the expansion into the inverse powers of the coordination number. The functions F_n are determined by the Hamiltonian of the system Eq. 1, or more precisely by the commutator with the reduced density matrix. Starting the iterative scheme to lowest order $\mathcal{O}(Z^0)$, the evolution equation for the on-site density matrix is given by $i\partial_t \hat{\rho}_\mu = F_1(\hat{\rho}_\mu, 0) + \mathcal{O}(1/Z)$. Its zeroth-order solution $\hat{\rho}_\mu^0$ yields the mean-field background as the starting point for the higher orders. For the sake of the Mott insulator description at half-filling and in the regime of large repulsion $U \gg T$, the mean-field *ansatz* we choose is

$$\hat{\rho}_\mu^0 = \frac{|\uparrow\rangle_\mu \langle\uparrow| + |\downarrow\rangle_\mu \langle\downarrow|}{2}. \quad (3)$$

There is one particle per site without any spin ordering. The semiconductor is represented by $\hat{\rho}_\mu^0 = |\uparrow\downarrow\rangle_\mu \langle\uparrow\downarrow|$ for the valence band and by $\hat{\rho}_\mu^0 = |0\rangle_\mu \langle 0|$ for the conduction

band (at zero temperature). Note that the two cases are related to each other via particle-hole duality. For more details see [23, 28].

B. Quasi-Particle Operators

To first order $\mathcal{O}(Z^{-1})$, the correlation functions obey $i\partial_t \hat{\rho}_{\mu\nu}^{\text{corr}} = F_2(\hat{\rho}_\mu^0, \hat{\rho}_{\mu\nu}^{\text{corr}}) + \mathcal{O}(1/Z^2)$ on top of the mean-field background. For a more detailed view see, e.g. [28–30].

To analyze the evolution of the quasi-particles it is beneficial to introduce the quasi-particle and hole operators

$$\hat{c}_{\mu s I} = \hat{c}_{\mu s} \hat{n}_{\mu \bar{s}}^I = \begin{cases} \hat{c}_{\mu s} (1 - \hat{n}_{\mu \bar{s}}) & \text{for } I = 0 \\ \hat{c}_{\mu s} \hat{n}_{\mu \bar{s}} & \text{for } I = 1 \end{cases}, \quad (4)$$

where \bar{s} denotes the spin state opposite to s . They create doublons ($I = 1$) or holons ($I = 0$). Note that these operators are approximately, but not exactly equal to the quasi-particle creation and annihilation operators for holons and doublons, see, e.g. [17]. The idea of such effective operators that better describe the physical excitations goes back to Hubbard X operators [35, 36] and composite operators [37].

In terms of these operators, we are able to write down the evolution equation for the correlation functions $\langle \hat{c}_{\mu s I}^\dagger \hat{c}_{\nu s J} \rangle^{\text{corr}}$. They consist of a homogeneous part coupling the different correlations and stationary source terms, that are not needed to describe the propagation of the quasi-particles. The source terms can be used to calculate ground state correlations. Moreover, it can be shown that the factorization

$$\langle \hat{c}_{\mu s I}^\dagger \hat{c}_{\nu s J} \rangle^{\text{corr}} = p_{\mu s I}^* p_{\nu s J}, \quad (5)$$

where the factors $p_{\nu s I}$ obey the simple equation

$$(i\partial_t - U_\mu^I - V_\mu) p_{\mu s I} = \frac{-1}{Z} \sum_{\nu J} T_{\mu\nu} \langle \hat{n}_{\mu \bar{s}}^I \rangle^0 p_{\nu s J}, \quad (6)$$

yields the same dynamics, for details see [23]. Furthermore, we assume a highly symmetric lattice such as a hyper-cubic one, to apply a Fourier transformation of the dependency parallel to the interfaces in the system. It reads

$$\begin{aligned} p_{\mu s I} &= \frac{1}{\sqrt{N^\parallel}} \sum_{\mathbf{k}^\parallel} p_{n, \mathbf{k}^\parallel, s}^I e^{i\mathbf{k}^\parallel \cdot \mathbf{x}_\mu^\parallel} \\ T_{\mu\nu} &= \frac{Z}{N^\parallel} \sum_{\mathbf{k}^\parallel} T_{m, n, \mathbf{k}^\parallel} e^{i\mathbf{k}^\parallel \cdot (\mathbf{x}_\mu^\parallel - \mathbf{x}_\nu^\parallel)}. \end{aligned} \quad (7)$$

and for isotopic nearest neighbor hopping $T_n^\parallel = T_{n, n-1}^\perp = T$ the components read

$$\begin{aligned} T_{m, n, \mathbf{k}^\parallel} &= \frac{T_{\mathbf{k}^\parallel}}{Z} \delta_{m, n} + \frac{T}{Z} (\delta_{n, n-1} + \delta_{n, n+1}) \\ T_{\mathbf{k}^\parallel}^\parallel &= 2T \sum_{x_i} \cos(p_{x_i}^\parallel) \equiv Z T_{\mathbf{k}}^\parallel, \end{aligned} \quad (8)$$

with the hopping contribution $T_{\mathbf{k}}^{\parallel}$. From Eq. 6 we read of that the different spin sectors decouple, therefore we drop the s and \mathbf{k}^{\parallel} indices for readability and find

$$(E - U_n^I - V_n) p_n^I + \langle \hat{n}_n^I \rangle^0 \sum_J T_{\mathbf{k}}^{\parallel} p_n^J = -T \frac{\langle \hat{n}_n^I \rangle^0}{Z} \sum_J (p_{n-1}^J + p_{n+1}^J), \quad (9)$$

where $n \in \mathbb{Z}$ now just labels the lattice sites perpendicular to the interface. These equations show a linear dependency of quasi-particle p_n^I and hole p_n^0 solutions in the Mott insulator while in the semiconductor one of them is identically zero, in the valence or conduction band, respectively.

In those regions of constant U_n or V_n we solve Eq. 9 by

$$p_n^I = \alpha^I e^{i\kappa n} + \beta^I e^{-i\kappa n}. \quad (10)$$

This yields an effective wave number κ perpendicular to the interface. The propagation within the semiconductor with a vanishing repulsion $U_n = 0$ and a constant on-site potential $V_n = V$, is governed by the effective wave number

$$\cos \kappa_{\text{semi}} = \frac{Z}{2T} [V - E - T_{\mathbf{k}}^{\parallel}]. \quad (11)$$

This is a band-like dispersion relation with $E = V - T_{\mathbf{k}}$. The Mott insulator, however, corresponds to a large constant on-site repulsion $U_n = U \gg T$ with a vanishing potential $V_n = 0$. In this case, the effective wave number reads

$$\cos \kappa_{\text{Mott}} = \frac{Z}{2T} \left[\frac{E(U - E)}{E - U/2} - T_{\mathbf{k}}^{\parallel} \right]. \quad (12)$$

The corresponding dispersion in the Mott insulator reads $E = \frac{1}{2} (U - T_{\mathbf{k}} \pm \sqrt{U^2 + T_{\mathbf{k}}^2})$ with the kinetic energy contribution $T_{\mathbf{k}} = T_{\mathbf{k}}^{\parallel} + \frac{2T}{Z} \cos \kappa_{\text{Mott}}$. This dispersion relation falls in line with the ones obtained by other methods like Hubbard-I [35], Roth's two pole approximation [38] or composite operator methods [39]. For more details about this and a comparison between the hierarchy of correlations and DMFT see [23].

In the strongly interacting regime $U \gg T$ considered here, real solutions for κ exist only for small $E \approx 0$ (lower Hubbard band) or for $E \approx U$ (upper Hubbard band).

The dispersion relations found above for the doublons and holons are the starting point to calculate their transmission through different types of heterostructures, made up either by different semiconductors or semiconductors and Mott insulators.

III. SEMICONDUCTOR HETEROSTRUCTURE

As proof of principle, we reproduce some well known results [5] using the hierarchy of correlations. We consider a pure semiconductor structure matching previous

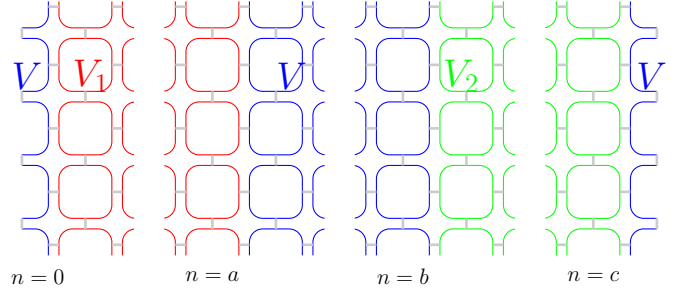


FIG. 1: (Color online) Schematic of the system; different semiconductors with potential V , V_1 and V_2 are combined to a heterostructure.

studies employing the transfer matrix method [5], which often involve superlattices with numerous wells. The schematic representation of our structure is presented in Fig. 1. There is one type of semiconducting material with on-site potential V functioning as the leads for sites $n \in (-\infty, 0]$ and $n \in [c + 1, \infty)$, as well as the connecting layer $n \in [a + 1, b]$. It connects two different layers with V_1 in $n \in [1, a]$ and V_2 in $n \in [b + 1, c]$. As mentioned, we assume an uniform hopping strength T across the entire lattice, although this restriction could be lifted straightforwardly. In the following analysis, the solution for the semiconductor given by Eq. 9 is denoted as $s_{\pm}^n = e^{\pm i\kappa_{\text{semi}} n}$, with the wavevector defined in Eq. 11. Additionally, $s_{j\pm}$, with $j = 1, 2$, provide the solution in the intermediate regions characterized by potentials V_1 and V_2 . Without normalization, the *ansatz* we use is

$$p_n^0 = \begin{cases} s_+^n + R s_-^n & n \leq 0, \\ A s_{1+}^n + B s_{1-}^n & 0 < n \leq a, \\ C s_+^n + D s_-^n & a < n \leq b, \\ E s_{2+}^n + F s_{2-}^n & b < n \leq c, \\ \mathcal{T} s_+^n & c < n, \end{cases} \quad (13)$$

as s_+ describes right propagating and s_- left propagating solutions. From Fig. 1 and Eq. 9 we read of boundary equations at the four interfaces and solve for the transmission amplitude \mathcal{T} (see App. VII A for the boundary conditions and the expression for the transmission amplitude).

The effective wave number Eq. 11 for the semiconducting layers shows that evanescent solutions have $|\kappa_s| \propto \ln V$. The stronger the band mismatch, the stronger the suppression of tunneling. In combination with the injected energy of the plane wave $E \in [V, V - T]$ and a sufficiently large filtering layer V_1 and V_2 , all energies $E > \min\{V_1, V_2\}$ get filtered out if $V_1, V_2 < V$. In Fig. 2, this is shown exemplarily for $V_1 = V_2 = 0.9V$ (dotted curve) and a fixed k^{\parallel} ; for $E < V_1$ there is nearly zero transmission. There are exponentially small tunnel currents. Otherwise, for $V_1 < V < V_2$ there might be an overlap in the bands around V_1 . Consequently, everything outside of this overlap gets filtered out, see solid

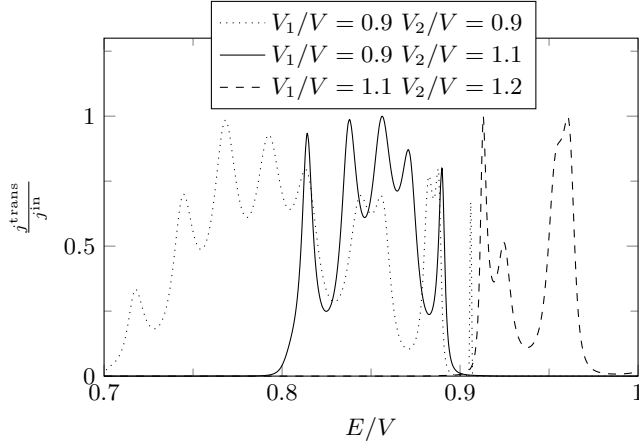


FIG. 2: Transmission as a function of electron energy through the semiconductor heterostructure of various band-offsets. We use $Z = 4$ for a two-dimensional problem and $T/V = 0.3$, $a = 7$, $b = 10$, $c = 17$. The band width of the “leads” is given by the plot range.

curve in Fig. 2. Using $V_1, V_2 > V$ on the other hand, everything below $E < \max\{V_1, V_2\} - T$ gets filtered out, see the dashed curve in the same figure. In all three difference scenarios, there are a lot of oscillations in the transmission. By including more and more structure to create a superlattice [5] these oscillations can be smoothed out and we would find real transmission minibands, because there is more constructive interference in these superlattices than in the small system here.

If the hopping is not isotropic, it is possible to achieve the same energy filtering with just two types of semiconductors. The filtering regions ought to have smaller hopping than the leads. This then results in symmetric transmission minibands. With isotropic hopping this system is only capable of filtering out energies above a certain value.

A. Smaller structure – non-isotropic hopping

As mentioned, in the case of non-isotropic hopping the energy filtering effect and minibands can be achieved by a structure consisting of only two different semiconductors; one acting as the leads and another one with smaller hopping as the gate. With a similar *ansatz* as for the bigger structure with s_{\pm} and m_{\pm} describing the solutions in the leads and the gate, respectively, we find the transmission amplitude

$$\mathcal{T} = \frac{(m^2 - 1)(s^2 - 1)m^{a+1}s^{-a-1}}{(ms - 1)^2 - m^{2a+2}(m - s)^2}. \quad (14)$$

It is exemplarily shown in Fig. 3 for sample parameters $V_m/V = 0.9$ and $T/T_m = 3$. By shifting the gate potential and thus the band overlap this setup can filter all energies above or below a certain energy or produce

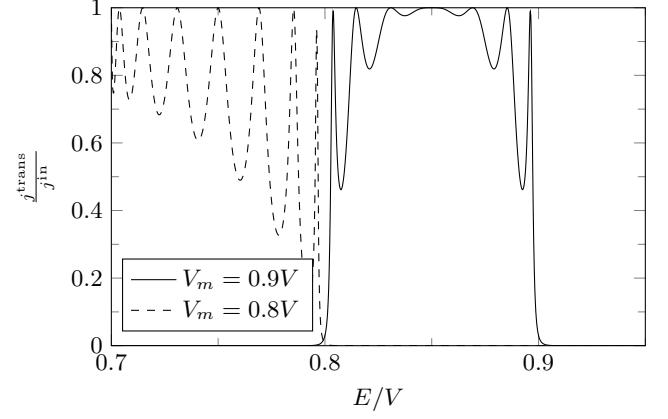


FIG. 3: Transmission as a function of energy through the structure with two types of semiconductors. We use $Z = 4$ for a two-dimensional problem and $T/V = 0.3$ and $a = 7$. The gate potential is $V_m/V = 0.9$ (solid) and $V_m/V = 0.8$ (dashed) and the hopping within the gate is $T_m/V = 0.1$.

transmission minibands. These can only be symmetric.

IV. MOTT-SEMICONDUCTOR STRUCTURE

Having successfully demonstrated our method for a well studied case of a semiconductor structure, our focus now shifts toward investigating a Mott insulator-semiconductor heterostructure. In this new configuration, semiconducting leads, serving as source and drain terminals, encase a Mott insulating material characterized by an on-site repulsion parameter denoted as U . Within this insulating region, there exists another semiconductor segment controlled by a gate voltage V_m . A schematic representation of this structure is provided in Fig. 4a. Fig. 4b shows the band edges of the lead, drain and gate relative to the Hubbard bands of the Mott insulating layers. Notably, the application of a gate voltage results in a shift of the (red) band within the middle region, denoted as $V_m - T_{\mathbf{k}}$, thereby modifying the transmission characteristics.

Again, we use a plane wave ansatz for the different semiconducting and the Mott insulating regions, the source and drain s_{\pm} , the Mott insulating layers r_{\pm} and the gate voltage region m_{\pm} . Hence, the *ansatz* is given by

$$p_n^0 = \begin{cases} s_+^n + R s_-^n & n \leq 0, \\ A r_+^n + B r_-^n & 0 < n \leq a, \\ C m_+^n + D m_-^n & a < n \leq b, \\ E r_+^n + F r_-^n, & b < n \leq c, \\ \mathcal{T} s_+^n & c < n. \end{cases} \quad (15)$$

The solutions in the various regions are in accordance to

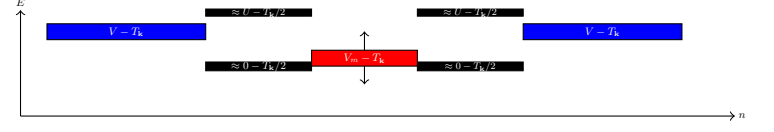
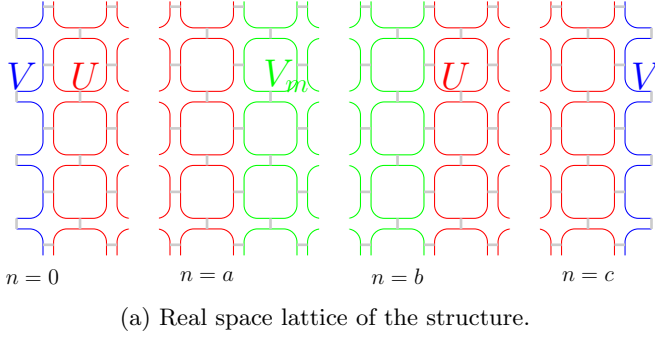


FIG. 4: One semiconductor with a gate voltage V_m between the same Mott insulating material U , everything is connected to a source and drain lead V .

Eqs. 16 and 12 and thus given by

$$s_{\pm} = e^{i\kappa_{\text{semi}}n}, \quad \cos \kappa_{\text{semi}} = \frac{Z}{2T} [V - E - T_{\mathbf{k}}^{\parallel}], \quad (16)$$

$$m_{\pm} = e^{i\kappa_m n}, \quad \cos \kappa_m = \frac{Z}{2T} [V_m - E - T_{\mathbf{k}}^{\parallel}], \quad (17)$$

$$r_{\pm} = e^{i\kappa_{\text{Mott}}n}, \quad \cos \kappa_{\text{Mott}} = \frac{Z}{2T} \left[\frac{E(U - E)}{E - U/2} - T_{\mathbf{k}}^{\parallel} \right]. \quad (18)$$

Due to the different structure the boundary conditions obtained from Eq. 9 change (see App. VII B). The transmission amplitude we find reads

$$\mathcal{T}(E, k^{\parallel}) = \frac{(m^2 - 1)(r^2 - 1)^2(s^2 - 1)(-m^{a+b})r^{a+b+c+1}}{s^{c+1}(W_1 + W_2)} \quad (19)$$

with long expressions W_1 and W_2 given in App. VII B. The transmitted current is given by the absolute square $|\mathcal{T}(E, k^{\parallel})|^2$ [23], because the leads have the same effective wave number.

A. Transmittance

In the current context, we can discern three primary scenarios. Firstly, the potential at the source and drain terminals, denoted as V , may fall below the lower Hubbard band. Alternatively, it could lie within the region between the two bands. Lastly, it might exceed the upper Hubbard band. Additionally, there is a possibility that the potential is (partially) situated within one of the two Mott bands. In this case, the presence of such a potential configuration results in the emergence of a transmission channel. The discussion can be simplified substantially by using the particle-hole symmetry [23] in the Mott insulating layers. The particle p_n^1 and hole p_n^0 solutions are related via $(E - U)p_n^1 = Ep_n^0$ which shows the symmetry around $U/2$, the middle of the band gap. Therefore, it is enough to look at three different cases: V below lower Hubbard band, V inside lower Hubbard band and V inside the Mott gap but below $U/2$. The other ones can

be obtained by the symmetry operation of inversion at the $U/2$ energy with appropriately shifting the on site potentials.

1. $V = -0.3U$ - below lower Hubbard band

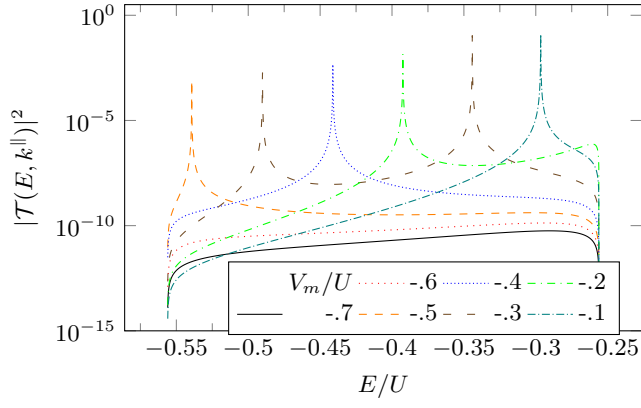
Using $V = -0.3U$ and a specific parallel momentum value k^{\parallel} , the transmittance exhibits a pronounced peak. This resonance energy shifts with the gate potential V_m . It is important to note that these resonant states do not manifest for all values of V_m . Instead, we observe them solely within a range of gate potentials $-0.4 < V_m/U < -0.2$ (Fig. 5a). The resonances only appear if there is a band overlap between the leads and the gate, as they stem from constructive interference within the gate region.

2. $V = 0U$ - lower Hubbard band

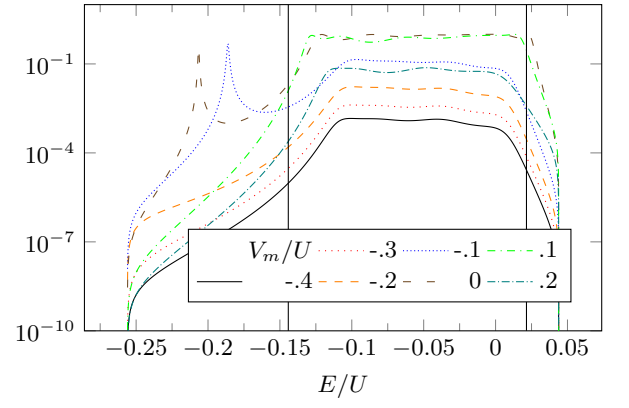
In the $V = 0U$ case, the lead bands cover the lower Hubbard band fully covered, but reach down further in energy. By varying the gate potential, V_m we find peaks below the lower Hubbard band, see Fig. 5b. Inside the lower Hubbard band there is a transmission channel with nearly constant transmission for all gate potentials; they only differ in the absolute value of the transmission. Above the band, transmission sharply drops off to zero (besides exponentially small tunneling currents).

3. $V = 0.3U$ & $V = 0.7U$ - inside Mott gap

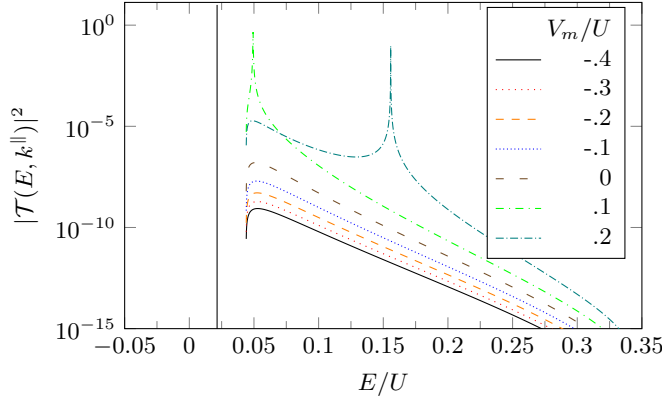
In [23], it was demonstrated that there is exactly zero transmission through Mott layers in the middle of the Mott gap $E = U/2$ with an unpolarized spin background, which is the case here. At this particular energy level, a perfect destructive interference between particle and hole currents occurs. Consequently, it is crucial to differentiate between situations where the energy is below or above this specific point. In Fig. 5c, we observe the



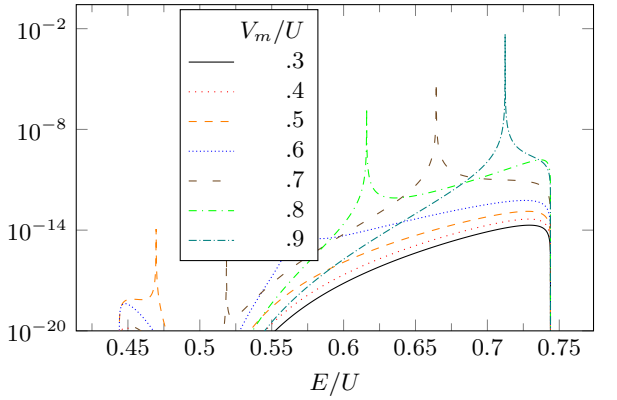
(a) (Color online) With $V = -0.3U$ the energy range is below the lower Hubbard band



(b) (Color online) With $V = 0U$ the lower Hubbard band is fully covered.



(c) (Color online) The electron energy is in between the two Hubbard bands, below the point $E = U/2$.



(d) (Color online) The electron energy is in between the two Hubbard bands, above the point $E = U/2$.

FIG. 5: Transmission for $k_{\parallel} = \pi/4$ through the semiconductor-Mott heterostructure as a function of electron energy for different on-site potentials relative to the Hubbard bands. The plot range always gives the band of the source/drain, the different colors depict different V_m/U . Vertical lines depict the Hubbard bands, if lying in the depicted range. The parameters are $T = 0.3U$, $Z = 4$, $a = 2$, $b = 5$, $c = 6$

first scenario, where the energy is below the midpoint of the band gap. Similar to previous observations, a peaked transmission structure is obtained for specific values of the gate potential V_m , while for other values, the transmission remains nearly constant close to zero.

For the second scenario, where the energy is above the midpoint of the band gap, refer to Fig. 5d. The symmetry between to two cases below and above the midpoint of the Mott gap can be seen.

B. Resonances

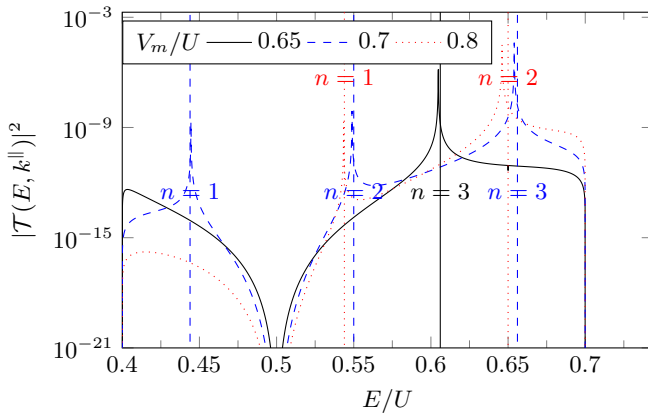
In the various scenarios discussed above, we observe peaks or resonances in the transmittance outside the Mott bands. Because of this, these resonances can only arise from constructive interference within the gate and should fulfill $\kappa_m d = n\pi$. Here, κ_m is the wave number, d is the thickness of the gate layer, and $n \in \mathbb{Z}$ is an integer.

These conditions lead to resonance energies E_{res} given by:

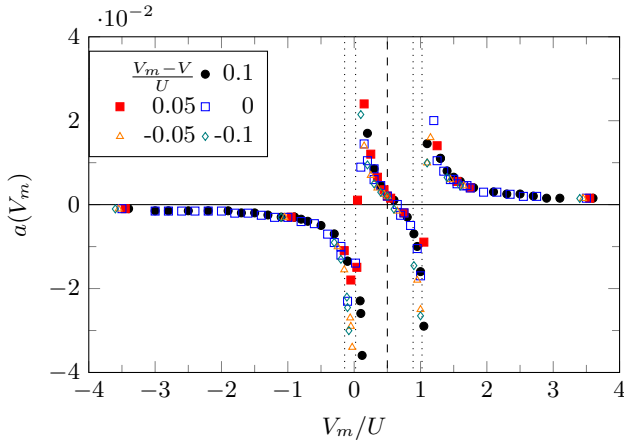
$$E_{\text{res}} = \frac{-2T \cos(k_{\parallel}) + V_m Z - 2T \cos(\frac{\pi n}{d})}{Z}. \quad (20)$$

However, when comparing these predicted resonance energies to the actual ones, $E_{\text{res}}^{\text{real}}$ obtained from $|T|^2$ (Fig. 6a), we notice discrepancies. Assuming the correctness of the resonance energy formula, we introduce a renormalized gate voltage $V_m^r = V_m + a(V_m)$. Here, if $a(V_m)$ is negative, it signifies a downward shift in the gate voltage. In Fig. 6b, we present $a(V_m)$ for different cases where $|V_m - V| \leq T$, ensuring an overlap between the source/drain and gate bands to maintain resonances. Several observations can be made:

a) If the energy falls inside one of the Mott bands, it opens up a transmission channel throughout the structure. Thus the effective width of the region wherein constructive interference happens is larger than the gate region. This renders the resonance energy formula Eq. 20



(a) (Color online) Transmittance vs. predicted resonance energies.



(b) (Color online) Renormalization parameter $a(V_m)$ of the gate voltage. The dashed line marks $U/2$, the dotted lines give the Mott bands.

FIG. 6: (a) gives the transmittance as function of energy for a lead potential $V = 0.7U$ together with the resonance energies predicted by Eq. 20 as dashed vertical lines for different gate potentials V_m . (b) gives the renormalization parameter $a(V_m)$ for different for various combinations of V and V_m . The parameters are $T = 0.3U$, $Z = 4$, $a = 2$, $b = 5$, $c = 6$, $k^\parallel = \pi/4$.

wrong, because there might be modes fitting in more than one region now. The renormalization $a(V_m)$ compensates for this effect.

b) Outside the Mott bands, where the thickness of the layer is solely given by the gate region, the renormalization pushes the effective gate potential V_m away from the bands. Below the lower band, it is pushed towards smaller values with $a(V_m) < 0$, while above the upper band, it is pushed towards larger values with $a(V_m) > 0$.

c) Between the two Mott bands, a change in sign occurs at $\approx U/2$ (the shift is due to $k^\parallel \neq 0$). Below this point, $a(V_m)$ is positive, while above it, $a(V_m)$ is negative. Inside the Mott gap the effective gate potential is pushed towards the middle of the gap.

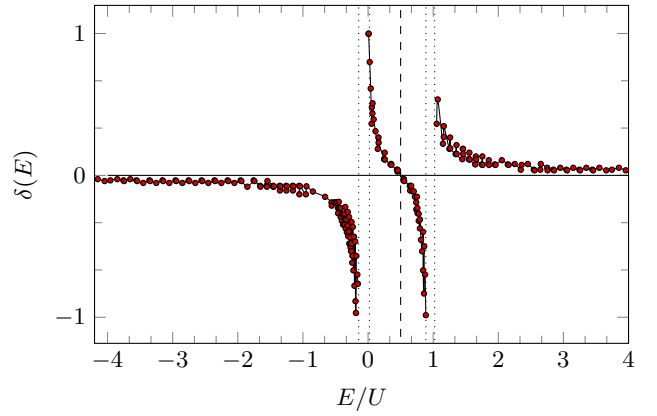


FIG. 7: (Color online) Phase shift $\delta(E)$ for $V = V_m$. The dashed line marks $U/2$, the dotted lines give the Mott bands.

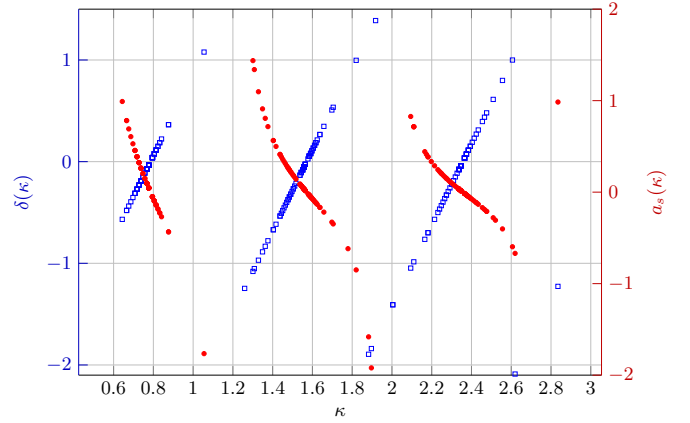


FIG. 8: (Color online) Phase shift $\delta(\kappa)$ (blue squares, left axis) and scattering length $a_s(\kappa)$ (red circles, right axis) for $V = V_m$. The oscillations are an artifact of the energy resolution used in the analysis.

Overall, these trends are consistent across different $V_m - V$ cases, with small deviations attributable to numerical considerations. Thus, there is no dependency on the specific distance $V_m - V$, and only the relative position of the gate voltage V_m with respect to the Mott bands is of significance. Far away from the bands the renormalization goes to zero $a(V_m \gg U) = a(V_m \ll 0) \rightarrow 0$.

C. Scattering Phase

In order to obtain the renormalized gate potential to explain the shift between the predicted and real resonances we need to assume the correctness assumed $\kappa_m d = n\pi$ to be valid. This is different for the phase accumulation model for quantum wells [40–42]: there, the scattering phase $\delta(E)$ modifies the resonance condition

to

$$\kappa_m d = n\pi + \delta(E). \quad (21)$$

This scattering phase is energy-dependent and leads to resonance energies described by

$$E_{\text{res}}^\delta = \frac{-2T \cos(k^\parallel) + V_m Z - 2T \cos\left(\frac{\pi n + \delta(E)}{d}\right)}{Z}. \quad (22)$$

From these resonance energies, we can deduce the behavior of the scattering phase, $\delta(E)$, as depicted in Figure 7. The energy range is covered by tuning the lead potential V . Notably, like the renormalization of the potential, the scattering phase undergoes a sign change at the Mott bands and at $U/2$. As one moves far away from the Mott bands, the scattering phase tends to zero. Functionally, the energy dependent scattering phase $\delta(E)$ depends on the band width contribution $W = \frac{2T}{Z}$ from the hopping orthogonal to the interfaces. With this, it reads

$$\delta(E) = \begin{cases} \frac{W}{2} \frac{1}{E + \frac{W}{2}} & E < \text{lower Hubbard band,} \\ -W \tan\left(\pi \left[\frac{E}{U} - \frac{U}{2}\right]\right) & \text{between Hubbard bands,} \\ \frac{W}{2} \frac{1}{E - U + \frac{W}{2}} & E > \text{upper Hubbard band.} \end{cases} \quad (23)$$

As expected, the maximum of the derivative of the scattering phase coincides with the Mott bands. This observation is in line with the fact that this quantity essentially describes the density of states [43].

From the scattering phase and the wave vector κ , we can also compute the scattering length $a_s(\kappa) = \frac{-\tan(\delta(\kappa))}{\kappa}$. Fig. 8 shows the scattering phase $\delta(\kappa)$ together with $a_s(\kappa)$. There are several branches of the momentum dependent scattering phase $\delta(k)$ (blue squares) that show a linear dependence on the wave number. For every branch the scattering length thus is given by $a_s(\kappa) \propto \tan(\text{const}_1 \kappa + \text{const}_2)/\kappa$ (red circles).

D. Parallel Momentum Integrated Transmission

In practical real-world setups, controlling the value of k^\parallel for electrons can be challenging. The electrons occupy all possible parallel momentum values, and in order to incorporate the fact that k^\parallel is not resolved, we will consider transmission probabilities that are averaged over k^\parallel , denoted as $\mathcal{T}(E)$:

$$\mathcal{T}(E) = \frac{1}{N} \int \mathcal{T}(E, k^\parallel) dk^\parallel. \quad (24)$$

The resulting transmittance represents a superposition of individual transmission probabilities, leading to a superposition of peaks in the transmission spectrum. Tuning the gate voltage V_m shifts the region of appreciable transmission to either lower or higher energies.

For example, when $V_m = 0.9U$ (Fig. 9a), we observe a shift towards higher energies in the transmission spectrum for $V = 0.7U$. Conversely, when V_m is adjusted

to $0.5U$, the transmission spectrum shifts towards lower energies. Also, the magnitude of the transmission goes down. Away from the occurring maximum transmittance, there is an exponential drop of.

Additionally, the higher peak in the transmission spectrum can also be shifted by varying the gate voltage, as demonstrated in Fig. 9c. In this case, transitioning from $V_m = 0.2U$ to $0.4U$ causes the highest transmission peak to shift followed by an exponential tail, here to higher energies. This exponential decay acts as the envelope of transmission peaks.

However, it is crucial to note that these observations primarily apply outside the Mott bands. Inside the Mott bands, changing the gate voltage tends to result in relatively flat transmission curves, as depicted in Fig. 9b. The alteration in gate voltage primarily affects the overall magnitude of transmission and the offset from zero outside the Mott bands.

E. Applying an Overall Voltage

Finally, we introduce a global voltage to the entire system. As depicted in Figure 10 there is a potential difference between the source V_S and the drain V_D creating the driving voltage. This alters the on-site potential in all the layers, also affecting the Mott layers. Fig. 10 shows a small applied voltage shifting the right Mott layer relative to the left one. Inside the layers, for simplicity, the potential is assumed constant. For small fractions of voltage over system size this seems reasonable. With more sophisticated methods to solve all the boundary equations (e.g. transfer matrices) this can easily be refined. Consequently, we find the transmittance $T(E)$ as

$$T(E) = |\mathcal{T}(E)|^2 \frac{\sin(\kappa_D)}{\sin(\kappa_S)}. \quad (25)$$

The additional factor $\frac{\sin(\kappa_D)}{\sin(\kappa_S)}$ comes because the effective wave numbers and thus the group velocities are not the same within the source and the drain.

Fig. 11 shows the transmission for some exemplary values of the source, drain and gate potential. The gate voltage can be used to tune the energy range of the transmission. This is true within the energy range of the Mott bands and outside.

V. CONCLUSIONS

In summary, we studied different types of heterostructures built by Mott insulators with on-site Coulomb repulsion U and semiconductors on-site potential V . The hierarchy-of-correlations approach allows us to treat the strongly interacting Mott insulators and the weakly interacting semiconductors within the same framework. Using this formal expansion into the inverse coordination number $1/Z$, we can assign effective wave vectors to the

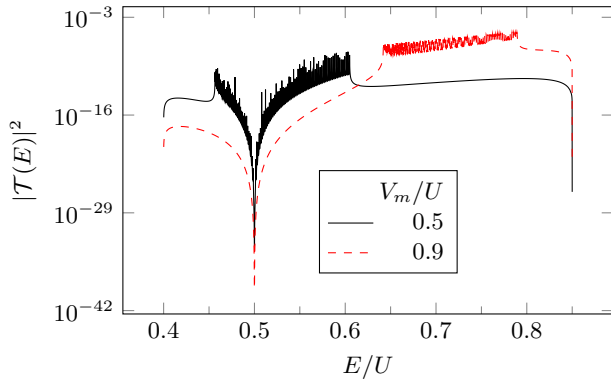
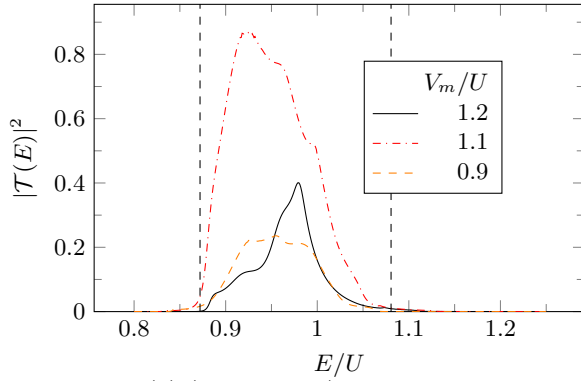
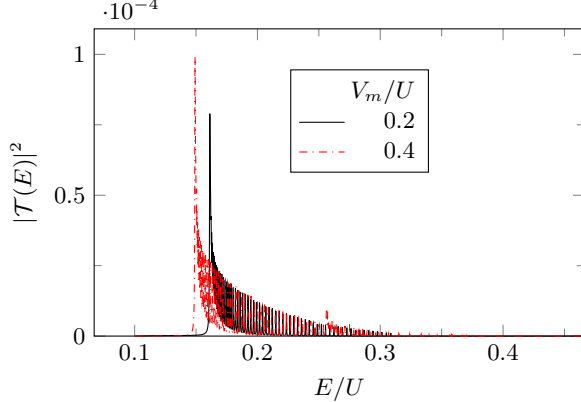
(a) (Color online) $V = 0.7U$ (b) (Color online) $V = 1.1U$ (c) (Color online) $V = 0.4U$

FIG. 9: Parallel momentum averaged transmittance for different source/drain potentials V as a function of electron energy. Dashed lines mark the edges of the upper Hubbard band. The parameters are $T = 0.3U$, $Z = 4$, $a = 2$, $b = 5$, $c = 6$.

quasi-particles allowing us to calculate the transmission probability through various types of structures with and without an applied voltage.

For a semiconductor structure, our approach reproduces the well-known result of transmission through minibands.

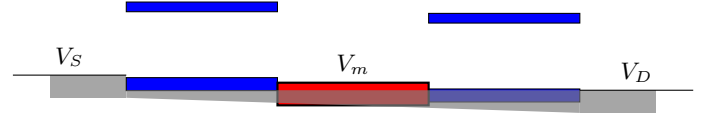


FIG. 10: “Band structure” of the system with applied voltage, the drain V_D is lower than the source V_S , the gate potential V_m is still adjustable. The applied voltage also shifts the Mott bands. Here, a linear behaviour is assumed while inside the distinctive regions the potential is taken to be constant.

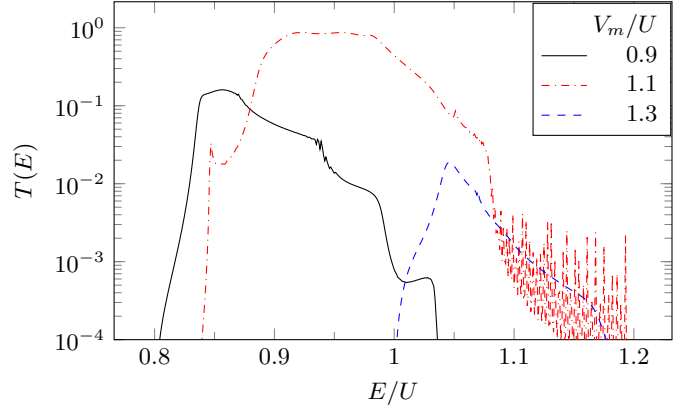


FIG. 11: Transmission through the semiconductor-Mott heterostructure with an applied voltage for a source potential $V_S = 1.1U$ and a drain potential $V_D = 0.7U$ as a function of energy for different gate potentials. The parameters are $T = 0.3U$, $Z = 4$, $a = 2$, $b = 5$, $c = 6$.

The Mott insulator-semiconductor heterostructure, on the other hand, allows us to make use of the strong suppression of the quasi-particle current due to destructive interference of the particle and hole channels in the middle of the Mott insulator band gap. Within a phase accumulation model for quantum wells we determine analytical expressions for the resonance energies which depend on the energy relative to the Mott bands.

Looking at the transmission curves integrated over parallel momentum, we find a skewness in the transmission function around its center that could have possible applications in thermoelectric devices. The energies for which transmission is found can be tuned by the gate. In this setting, the skewness of the transport distribution function is desirable as it helps to increase the Seebeck coefficient [16]. This feature distinguishes heterostructures with a Mott insulator, i.e., with strongly interacting electrons, from a pure semiconductor structure.

VI. ACKNOWLEDGEMENT

The authors thank F. Queisser and R. Schützhold for fruitful discussions and valuable feedback on the

manuscript. Funded by the Deutsche Forschungsgemeinschaft (DFG, German Research Foundation) – Project-ID 278162697– SFB 1242.

VII. APPENDIX

A. Semiconductor Structure

From Eq. 9 we can deduct two boundary equations per interface for the structure shown in Fig. 1. One for the lattice site left of the interface and one to the right of it. In this case the eight equations read (after some algebra)

$$s_{1+}B + \frac{A}{s_{1+}} = \left(\frac{1}{s_+} + Rs_+ \right) \quad (26)$$

$$1 + R = (A + B) \quad (27)$$

$$As_{1+}^{a+1} + \frac{B}{s_{1+}^{a+1}} = \left(Cs_{1+}^{a+1} + \frac{D}{s_{1+}^{a+1}} \right) \quad (28)$$

$$Cs_{1+}^a + \frac{D}{s_{1+}^a} = \left(As_{1+}^a + \frac{B}{s_{1+}^a} \right) \quad (29)$$

$$Cs_{1+}^{b+1} + \frac{D}{s_{1+}^{b+1}} = \left(sr_{2+}^{b+1} + \frac{F}{s_{2+}^{b+1}} \right) \quad (30)$$

$$Es_{2+}^b + \frac{F}{s_{2+}^b} = \left(Cs_{1+}^b + \frac{D}{s_{1+}^b} \right) \quad (31)$$

$$Es_{2+}^{c+1} + \frac{F}{s_{2+}^{c+1}} = \mathcal{T}s_{1+}^{c+1} \quad (32)$$

$$\mathcal{T}s_{1+}^c = \left(Es_{2+}^c + \frac{F}{s_{2+}^c} \right). \quad (33)$$

Inserting the *ansatz* 13 into this we can solve for the transmission coefficient behind the interface as

$$\mathcal{T} = \frac{-s_{1+}^{a+1} (s_{1+}^2 - 1) (s_{2+}^2 - 1) (s_+^2 - 1)^2 s_{1+}^{a+b} s_{2+}^{b+c}}{s_{1+}^{1+c} (M_1 + M_2 + M_3 + M_4 + M_5 + M_6)} \quad (34)$$

with the six terms

$$M_1 = s_{2+}^{2b} (s_{1+}^{2a} (s_{1+}^{2a+2} (s_{1+} - s_+)^2 - (s_{1+}s_+ - 1)^2) - (s_{1+}^{a+1} - 1) (s_{1+}^{a+1} + 1) s_{1+}^{2b+1} (s_{1+} - s_+) (s_{1+}s_+ - 1)), \quad (35)$$

$$M_2 = s_+ s_{2+}^{2b+2} (s_{1+}^{2a+1} (s_{1+}^{2a+2} (s_{1+} - s_+)^2 - (s_{1+}s_+ - 1)^2) - (s_{1+}^{a+1} - 1) (s_{1+}^{a+1} + 1) s_{1+}^{2b} (s_{1+} - s_+) (s_{1+}s_+ - 1)), \quad (36)$$

$$M_3 = s_{2+}^{2c+1} (2s_{1+}^{2a+1} (s_{1+}^{2a+2} (s_{1+} - s_+)^2 - (s_{1+}s_+ - 1)^2) - (s_{1+}^2 + 1) (s_{1+}^{a+1} - 1) (s_{1+}^{a+1} + 1) s_{1+}^{2b} (s_{1+} - s_+) (s_{1+}s_+ - 1)), \quad (37)$$

$$M_4 = s_{2+}^{2c+2} ((s_{1+}^{a+1} - 1) (s_{1+}^{a+1} + 1) s_{1+}^{2b+1} (s_{1+} - s_+) (s_{1+}s_+ - 1) + s_{1+}^{2a} ((s_{1+}s_+ - 1)^2 - s_{1+}^{2a+2} (s_{1+} - s_+)^2)), \quad (38)$$

$$M_5 = s_+ s_{2+}^{2c} ((s_{1+}^{a+1} - 1) (s_{1+}^{a+1} + 1) s_{1+}^{2b} (s_{1+} - s_+) (s_{1+}s_+ - 1) + s_{1+}^{2a+1} ((s_{1+}s_+ - 1)^2 - s_{1+}^{2a+2} (s_{1+} - s_+)^2)), \quad (39)$$

$$M_6 = s_{2+}^{2b+1} ((s_+^2 + 1) (s_{1+}^{a+1} - 1) (s_{1+}^{a+1} + 1) s_{1+}^{2b} (s_{1+} - s_+) (s_{1+}s_+ - 1) + 2s_{1+}^{2a+1} ((s_{1+}s_+ - 1)^2 - s_{1+}^{2a+2} (s_+ - s_+)^2)). \quad (40)$$

The transmission probability is given by the absolute square $|\mathcal{T}|^2$, because the two leads have the same effective wave number.

B. Mott–Semiconductor Structure with Single Gate

For the heterostructure combining the two Mott insulating regions U with the gate V_m (see Fig. 4a) the boundary conditions change. In the case of a half-filled background we find from Eq. 9 the eight equations

$$\begin{aligned} \tilde{B}r_+ + \tilde{A}r_+^{-1} &= Rs_+ + s_+^{-1}, \\ 1 + R &= \tilde{A} + \tilde{B}, \\ \tilde{A}r_+^{a+1} + \tilde{B}r_+^{-(a+1)} &= Cm_+^{a+1} + Dm_+^{-(a+1)}, \\ Cm_+^a + Dm_+^{-a} &= \tilde{A}r_+^a + \tilde{B}r_+^{-a}, \\ \tilde{E}r_+^b + \tilde{F}r_+^{-b} &= Cm_+^b + Dm_+^{-b}, \\ \tilde{E}r_+^{c+1} + \tilde{F}r_+^{-(c+1)} &= \mathcal{T}s_{1+}^{c+1}, \\ \mathcal{T}s_{1+}^c &= \tilde{E}r_+^c + \tilde{F}r_+^{-c}, \\ Cm_+^{b+1} + Dm_+^{-(b+1)} &= \tilde{E}r_+^{b+1} + \tilde{F}r_+^{-(b+1)}. \end{aligned} \quad (41)$$

where we introduced the abbreviations $\{\tilde{A}, \tilde{B}, \tilde{E}, \tilde{F}\} = \frac{E-V-U/2}{E-U-V} \{A, B, E, F\}$. Inserting the *ansatz* 15 yields the transmission amplitude

$$\mathcal{T}(E, k_{\parallel}) = \frac{(m^2 - 1) (r^2 - 1)^2 (s^2 - 1) (-m^{a+b}) r^{a+b+c+1}}{s^{c+1} (W_1 + W_2)}. \quad (42)$$

In this, the two long expressions read

$$\begin{aligned}
W_1 = & - \left(m^{2a} (r^{2a+3}(r-s) + rs - 1) (r^{2b}(rs-1) + r^{2c+1}(r-s)) \right. \\
& - rm^{2a+2} (r (r^{2a}(r-s) + s) - 1) (r^{2b+1}(rs-1) + r^{2c}(r-s)) \\
& + rm^{2b} (r (r^{2a}(r-s) + s) - 1) (r^{2b+1}(rs-1) + r^{2c}(r-s)) \\
& \left. + m^{2b+2} (r^{2a+3}(r-s) + rs - 1) (r^{2b}(rs-1) + r^{2c+1}(r-s)) \right) \\
W_2 = & m^{2a+1} (r^{2b+1}(rs-1) ((r^2+1)r^{2a+1}(r-s) + 2rs - 2) + r^{2c}(r-s) (2r^{2a+3}(r-s) + (r^2+1)(rs-1))) \\
& + m^{2b+1} (r^{2b+1}(rs-1) (-((r^2+1)r^{2a+1}(r-s)) - 2rs + 2) - r^{2c}(r-s) (2r^{2a+3}(r-s) + (r^2+1)(rs-1)))
\end{aligned} \tag{43}$$

-
- [1] Z. Lu, D. Lockwood, and J.-M. Baribeau, *Nature* **378**, 258 (1995).
- [2] M. Willatzen, R. V. Melnik, C. Galeriu, and L. L. Y. Voon, *Mathematics and Computers in Simulation* **65**, 385 (2004).
- [3] J. Liu, S. Okamoto, M. Van Veenendaal, M. Kareev, B. Gray, P. Ryan, J. Freeland, and J. Chakhalian, *Physical Review B* **83**, 161102 (2011).
- [4] T. Gaylord and K. Brennan, *Applied physics letters* **53**, 2047 (1988).
- [5] Q. Yang and A. Li, *Journal of Applied Physics* **87**, 1963 (2000).
- [6] H.-H. Tung and C.-P. Lee, *IEEE journal of quantum electronics* **32**, 2122 (1996).
- [7] J. Smoliner, R. Heer, and G. Strasser, *Surface and Interface Analysis: An International Journal devoted to the development and application of techniques for the analysis of surfaces, interfaces and thin films* **27**, 542 (1999).
- [8] A. Kan'an, A. Puri, and T. Odagaki, *Journal of applied physics* **74**, 370 (1993).
- [9] H.-H. Tung and C.-P. Lee, *IEEE Journal of Quantum Electronics* **32**, 507 (1996).
- [10] L. Whitlow and T. Hirano, *Journal of Applied Physics* **78**, 5460 (1995).
- [11] C. Summers and K. Brennan, *Applied physics letters* **48**, 806 (1986).
- [12] P. Harness, R. Pritchard, B. Khamsehpour, W. Truscott, and K. Singer, *Journal of applied physics* **71**, 3019 (1992).
- [13] C. Gayner and Y. Amouyal, *Advanced Functional Materials* **30**, 1901789 (2020).
- [14] N. Neophytou and M. Thesberg, *Journal of Computational Electronics* **15**, 16 (2016).
- [15] Y. Mune, H. Ohta, K. Koumoto, T. Mizoguchi, and Y. Ikuhara, *Applied Physics Letters* **91**, 192105 (2007).
- [16] J.-C. Zheng, *Research* 2022;2022:9867639 (2022).
- [17] I. Avigo, F. Queisser, P. Zhou, M. Ligges, K. Rossnagel, R. Schützhold, and U. Bovensiepen, *Physical Review Research* **2**, 022046 (2020).
- [18] J. Hubbard, *Proceedings of the Royal Society of London. Series A. Mathematical and Physical Sciences* **276**, 238 (1963).
- [19] B. Brandow, *Advances in Physics* **26**, 651 (1977).
- [20] V. I. Anisimov, J. Zaanen, and O. K. Andersen, *Physical Review B* **44**, 943 (1991).
- [21] P. A. Lee, N. Nagaosa, and X.-G. Wen, *Reviews of modern physics* **78**, 17 (2006).
- [22] L. Ju, T. Ren, Z. Li, Z. Liu, C. Shi, Y. Liu, S. Hong, J. Wu, H. Tian, Y. Zhou, *et al.*, *Physical Review B* **105**, 024516 (2022).
- [23] J. Verlage, F. Queisser, N. Szpak, J. König, P. Kratzer, and R. Schützhold, *International Journal of Theoretical Physics* **63**, 1 (2024).
- [24] M. C. Qian, C. Y. Fong, K. Liu, W. E. Pickett, J. E. Pask, and L. H. Yang, *Phys. Rev. Lett.* **96**, 027211 (2006).
- [25] Y.-C. Lin, Y. Chen, A. Shailos, and Y. Huang, *Nano Letters* **10**, 2281 (2010), pMID: 20499889, <https://doi.org/10.1021/nl101477q>.
- [26] S. Okamoto and A. J. Millis, *Physical Review B* **70**, 241104 (2004).
- [27] S. Okamoto, *Physical Review B* **76**, 035105 (2007).
- [28] F. Queisser, K. V. Krutitsky, P. Navez, and R. Schützhold, *Physical Review A* **89**, 033616 (2014).
- [29] P. Navez and R. Schützhold, *Physical Review A* **82**, 063603 (2010).
- [30] F. Queisser and R. Schützhold, *Physical Review A* **100**, 053617 (2019).
- [31] D. P. Arovas, E. Berg, S. A. Kivelson, and S. Raghu, *Annual review of condensed matter physics* **13**, 239 (2022).
- [32] M. Qin, T. Schäfer, S. Andergassen, P. Corboz, and E. Gull, *Annual Review of Condensed Matter Physics* **13**, 275 (2022).
- [33] L. D. Landau, *Sov. Phys. JETP* **3**, 920 (1957).
- [34] V. Solov'yev and I. Kukushkin, *Physical Review B* **96**, 115131 (2017).
- [35] J. Hubbard, *Proceedings of the Royal Society of London. Series A. Mathematical and Physical Sciences* **285**, 542 (1965).
- [36] S. G. Ovchinnikov and V. V. Val'kov, *Hubbard operators in the theory of strongly correlated electrons* (World Scientific, 2004).
- [37] F. Mancini and A. Avella, *Advances in Physics* **53**, 537 (2004).
- [38] L. M. Roth, *Physical Review* **184**, 451 (1969).
- [39] A. Avella, *The European Physical Journal B* **87**, 1 (2014).
- [40] A. Shikin, D. Vyalikh, G. Prudnikova, and V. Adamchuk, *Surface science* **487**, 135 (2001).
- [41] N. V. Smith, *Physical Review B* **32**, 3549 (1985).
- [42] A. Danese and R. Bartynski, *Physical Review B* **65**, 174419 (2002).
- [43] M. Davy, Z. Shi, J. Wang, X. Cheng, and A. Z. Genack, *Phys. Rev. Lett.* **114**, 033901 (2015).